Coenzyme binding and hydride transfer in *Rhodobacter capsulatus* ferredoxin/flavodoxin NADP(H) oxidoreductase

Ana Bortolotti[a#], Inmaculada Pérez-Dorado[b#], Guillermina Goñi[c], Milagros Medina[c], Juan A. Hermoso[b], Néstor Carrillo[a] and Néstor Cortez[a*]

[a]Instituto de Biología Molecular y Celular de Rosario, CONICET & Universidad Nacional de Rosario, Suipacha 531, S2002LRK Rosario, Argentina

[b]Grupo de Cristalografía Macromolecular y Biología Estructural, Instituto de Química-Física Rocasolano C.S.I.C., Serrano 119, 28006 Madrid, Spain

[c]Departamento e Bioquímica y Biología Molecular y Celular, Facultad de Ciencias, and BIFI, Universidad de Zaragoza, 50009 Zaragoza, Spain

[#] A. B. and I. P.-D. contributed equally to the manuscript and both should be considered as first auhor.

* *Corresponding author*: Néstor Cortez,

IBR, Área Biología Molecular

Facultad de Cs. Bioquímicas y Farmacéuticas, U.N.R.

Suipacha 531, S2002LRK Rosario, Argentina

TE: (54) (341) 435 0661/0596,

FAX: (54) (341) 439 0465

Email: cortez@ibr.gov.ar

Keywords: ferredoxin(flavodoxin)-NADP(H) oxidoreductase; *Rhodobacter capsulatus*; hydride transfer; coenzyme binding; $NADP^+$-complex structure

Abbreviations used: FNR plastidic ferredoxin NADP(H) oxidoreductase

FPR bacterial ferredoxin/flavodoxin NADP(H) oxidoreductase

Summary

Ferredoxin-NADP(H) reductases catalyse the reversible hydride/electron exchange between NADP(H) and ferredoxin/flavodoxin, comprising a structurally defined family of flavoenzymes with two distinct subclasses. Those present in Gram-negative bacteria (FPRs) display turnover numbers of 1-5 s^{-1} while the homologues of cyanobacteria and plants (FNRs) developed a 100-fold activity increase. We investigated nucleotide interactions and hydride transfer in *Rhodobacter capsulatus* FPR comparing them to those reported for FNRs. NADP(H) binding proceeds as in FNRs with stacking of the nicotinamide on the flavin, which resulted in formation of charge-transfer complexes prior to hydride exchange. The affinity of FPR for both NADP(H) and 2'-P-AMP was 100-fold lower than that of FNRs. The crystal structure of FPR in complex with 2'-P-AMP and $NADP^+$ allowed modelling of the adenosine ring system bound to the protein, whereas the nicotinamide portion was either not visible or protruding toward solvent in different obtained crystals. Stabilising contacts with the active site residues are different in the two reductase classes. We conclude that evolution to higher activities in FNRs was partially favoured by modification of NADP(H) binding in the initial complexes through changes in the active site residues involved in stabilisation of the adenosine portion of the nucleotide and in the mobile C-terminus of FPR.

Introduction

Ferredoxin-NADP(H) reductases (FNR, EC 1.18.1.2) are FAD-containing enzymes that catalyse the reversible electron transfer between one molecule of NADP(H) and two molecules of the low-potential electron carrier proteins ferredoxin (Fd) or flavodoxin (Fld) [1-6]. The overall reaction can be divided into a hydride transfer step between NADP(H) and FAD and an electron exchange reaction between FAD and the electron transfer protein partner.

FNRs are highly specific for NADP(H), displaying only marginal activity with NAD(H) [7, 8]. Flavoenzymes of this type are found in Gram-negative bacteria, cyanobacteria, apicoplasts, plant chloroplasts and non-photosynthetic plastids, where they participate in several key metabolic pathways including photosynthesis, nitrogen fixation, sulphur assimilation and amino acid synthesis [5]. The three-dimensional structures of several FNRs from plastids [9-15], cyanobacteria [16], eubacteria [17-21] and parasite apicoplasts [22] have been determined at 2 Å resolution or below, revealing a common structural framework made up of two well-defined domains. The N-terminal domain consists of a six stranded antiparallel β-barrel which accommodates the flavin molecule on its internal face, whereas the C-terminal domain displays a variation of the typical Rossmann fold responsible for pyridine nucleotide binding [9, 16, 17, 23]. Catalysis occurs in a crevice formed at the interphase between the two domains (reviewed in Carrillo & Ceccarelli) [2]. Comparison of the atomic structures helped to define these reductases as a distinct family, different from other flavoenzymes with FNR activity present in mitochondria or in Gram-positive bacteria [24, 25], and fuelled the rational use of site-directed mutagenesis to investigate the catalytic mechanism (reviewed in Medina & Gómez Moreno) [3]. They also showed that the two-domain structure of

FNR is the prototype for a larger family of flavin-containing electron transferases that includes nitric oxide synthase and cytochrome *P-450* reductase [26].

A closer inspection of the FNRs from different organisms revealed that although all members of the family derive from a common ancestor related to flavin reductases [27], they can be divided into two classes displaying significant structural differences, a result anticipated by sequence alignment analysis [5]. The reductases present in plastids and cyanobacteria are characterised by an extended conformation of the FAD molecule held in position by an extra loop in the N-terminal domain, and an invariant tyrosine residue at the C-terminus that shields the isoalloxazine ring system from solvent. In contrast, the enzymes from heterotrophic prokaryotes, including those found in bacteria exhibiting anoxygenic photosynthesis, lack the extra loop and consequently bind FAD in a bent conformation [17-21]. The architecture of the C-terminal region in the reductases of this bacterial-type class is also different. The amino acid facing the flavin is not the C-terminal residue and may be aromatic or aliphatic [5]. To acknowledge the distinctive features of the two reductase classes, the name FNR has been restricted to the plastidic/cyanobacterial/apicomplexan enzymes, while those found in eubacteria are termed FPRs.

Structural differences between FNRs and FPRs are somehow translated into catalytic efficiency. The bacterial-class reductases, which are presumably older, display activities in the range of 1-5 s^{-1}. With the advent of oxygenic photosynthesis in the primitive cyanobacteria and the concomitant recruitment of FNR for photosynthetic electron transport, these enzymes underwent a formidable increase in catalytic competence to cope with the high demands of the novel metabolism, with turnover numbers raising to 200-500 s^{-1} (reviewed in Carrillo & Ceccarelli [2]; Ceccarelli *et al.* [5]). The

modifications in the protein structure that account for these changes are largely unknown.

The mode and affinity of the interactions with the pyridine nucleotide must be necessarily different in the two classes of reductases, following the alterations undergone at the C-terminal stretch, even though the rate-limiting step for the overall process in both FNRs [28] and FPRs [19] appears to be the electron transfer reaction between FAD and Fd/Fld. Indeed, both single turnover [19, 29] and steady-state measurements [30, 31] showed that hydride transfer rates are at least 5-fold higher in FNRs, indicating that this half-reaction is also hampered in the bacterial-class enzymes.

Another structural change must take place during turnover in the FNR from plastids and cyanobacteria, as the phenol ring of the invariant C-terminal tyrosine must swing away to allow entrance of the nicotinamide for efficient hydride transfer [10, 23]. Although this tyrosine is not an absolute requirement for activity, it modulates several properties of the catalytic process, including preference of NADP(H) over NAD(H), degree of nicotinamide occupation on the flavin site in the productive complex, stabilisation of FAD semiquinone, midpoint redox potential and decrease of coenzyme affinity to levels compatible with steady-state turnover [32-34]. It also contributes significantly to holoenzyme stability [34, 35]. While this residue is strictly conserved in all plant, cyanobacterial and apicoplastic FNRs, requirements at the corresponding site in FPRs appears to be less stringent, admitting different types and numbers of amino acids [5]. For instance, the reductase from *Rhodobacter capsulatus* has an alanine at a position equivalent to the C-terminal tyrosine found in FNRs, followed by a stretch of five additional amino acids [19].

The purpose of the present research was to investigate the features of NADP(H) interaction with *R. capsulatus* FPR by applying binding equilibria analysis, rapid kinetic

measurements and X-ray crystallography. Our results indicate that the nicotinamide ring stacks on the flavin as in the plastidic enzymes, as revealed by the spectral perturbations elicited upon binding of both $NADP^+$ and NADPH to oxidised FPR, but dissociation constants were 20-fold higher in the *R. capsulatus* enzyme. Analysis of the crystal structure of FPR in complex with nucleotides allowed modelling of the 2'-P-AMP portion of NADP(H), which appears displaced 2.5 Å from the correspondent position in the plastidic enzymes showing different contacts with the protein residues of the two classes of reductases. For the first time in the bacterial type reductases, three different crystal forms for $NADP^+$ and one for 2'-P-AMP were obtained. Our results show that coenzyme docking occurred through the 2'-P-AMP moiety, and point to displacement of the protein C-terminus as a likely requirement to achieve a productive complex. We conclude that the increase in enzyme turnover experienced during the transition from FPR to FNR was largely attained by more efficient binding of NADP(H) in the initial Michaelis-Menten complex, while subsequent steps of transition-state formation and hydride transfer were hardly modified.

Materials and methods

Spectral analysis

Recombinant *R. capsulatus* FPR was purified from cleared lysates of *Escherichia coli* BL21(DE3) transformants using NTA (Quiagen) affinity chromatography, essentially as described before [31]. Absorption spectra were recorded on a Shimadzu UV-2450 spectrophotometer. Titrations of FPR_{ox} with $NADP^+$, 2'-P-AMP and NAD^+ were performed spectrophotometrically at 25 °C. The enzyme was diluted to a final concentration of 20 μM in 50 mM Tris-HCl, pH 8. Difference spectra were computed by subtracting from each spectrum that obtained in the absence of ligand, after correction for dilution. Dissociation constants (K_d) values were obtained by fitting data

sets to the equation of a rectangular hyperbola using SIGMAPLOT (Systat Software Inc., Point Richmond, CA).

Crystallisation and data collection

Complexes of FPR with $NADP^+$ and 2'-P-AMP were obtained by co-crystallisation using the hanging drop vapour diffusion method. Droplets were equilibrated against 500 µl of well solution at 18 °C. Crystals of the FPR-$NADP^+$ complex grew in 10-µl droplets giving three distinct forms which were referred to as Forms I, II and III. Crystals of Form I belong to the trigonal $P3_121$ space group and display the following unit cell dimensions: $a = b = 68.72$ Å, $c = 128.15$ Å. Crystals of Form II also belong to the trigonal $P3_121$ space group but exhibit different unit cell dimensions: $a = b = 61.92$ Å, $c = 123.0$ Å. Form III consists of monoclinic crystals which belong to the $P2_1$ space group and posses the following unit cell parameters: $a = 69.38$ Å, $b = 93.45$ Å, $c = 104.94$ Å, $\alpha = \gamma = 90.0^o$, $\beta = 89.97^o$. The three forms grew in the same precipitant solution formed by 20-26 % (w/v) PEG 3350 and 0.1 M sodium citrate, pH 5.5, in the presence of n-heptyl-β-D-thioglucoside (HTG). Form II grew in droplets formed by mixing 4 µl of a 6.9mg/ml protein solution buffered with 50 mM Tris-HCl, pH 8.0, 1 µl of an unbuffered 300 mM HTG solution, 1 µl of an unbuffered 20 mM $NADP^+$ solution and 4 µl of the precipitant solution. On the other side, forms I and III co-existed in the same droplets after mixing 4 µl of a 30 mg/ml original protein solution with the precipitant mixture. Crystals grew in 2-4 days reaching a maximum size of 0.4x0.4x0.4 mm (Form I), 0.15x0.15x0.2 mm (Form II) and 0.05x0.05x0.6 mm (Form III).

Crystals of FPR in complex with 2'-P-AMP consisted of hexagonal prisms which belong to the trigonal $P3_121$ space group. They were obtained using the same precipitant solution as in the case of the $NADP^+$ complexes and also in the presence of

HTG. Crystals grew in 5-μl droplets formed by mixing 2 μl of a 6.9 mg/ml protein solution buffered with 50 mM Tris-HCl, pH 8.0, 0.5 μl of an unbuffered 300 mM HTG solution, 0.5 μl of an unbuffered 40 mM 2'-P-AMP solution and 2 μl of the precipitant solution. Crystals reached their maximum size of 0.2x0.2x0.6 mm in 2-3 days.

An X-ray data set was collected for each of the different crystalline forms of FPR in complex with 2'-P-AMP and $NADP^+$. Measurements were done using synchrotron radiation as well as the graphite monochromated CuKα radiation as X-ray sources. Measurements carried out using synchrotron radiation were achieved in the ID14-2 and ID14-4 beam lines at the ESRF (European Synchrotron Radiation Facility at Grenoble, France). CuKα radiation was generated by an Enraf-Nonius rotating anode generator. Data sets were processed and scaled with the MOSFLM [36] and SCALA programmes from the CCP4 package [37].

Structural determination and refinement

All structures obtained for FPR in complex with $NADP^+$ and 2'-P-AMP were solved by the Molecular Replacement method using the MOLREP programme [38], on the basis of the free FPR structure (PDB code 2bgi). In all cases, unique and unambiguous solutions for the rotation and translation functions were obtained. Two of the complexes with $NADP^+$, Forms I and II, and the complex with 2'-P-AMP contained a unique molecule in the asymmetric unit, while the Form III $NADP^+$ complex displayed four molecules in the asymmetric unit. All crystallographic models were subjected to alternated cycles of refinement with the CNS programme [39] and manual model building with the package O software [40]. The good quality of the final electron density maps allowed us to model most of the residues of the 272-residues polypeptide chain: 257 amino acids in Form I (residues 16-272), 260 amino acids in Form II

(residues 13-272), 257 and 254 amino acids in Form III (residues 16-272 of chains A and C and residues 16-269 of chains B and D), and 257 amino acids in the 2'-P-AMP complex (residues 16-272). In all cases, one FAD and one $NADP^+$/2'-P-AMP molecule were found bound to each FPR molecule and, except in the case of Form III, one detergent molecule was observed bound to the enzyme (Table 1). The quality of the final geometry was checked with the PROCHECK [41] and WATCHECK programmes [42]. Statistics for refinement and model composition are summarised in Table 1. All figures of the crystallographic models were generated using the PYMOL programme [43].

Atomic coordinates and structure factors of FPR in complex with $NADP^+$ and 2'-P-AMP have been deposited in the PDB with the following accession codes: 2vnj ($NADP^+$ complex, Form I), 2vnh ($NADP^+$ complex, Form II), 2vnk ($NADP^+$ complex, Form III) and 2vni (2'-P-AMP complex).

Stopped-flow pre-steady-state kinetic measurements

Anaerobic fast kinetic reactions of FPR_{ox} with NADPH were followed using an Applied Photophysics SF.17MV stopped-flow. All buffers and samples were made oxygen-free. Changes in absorbance were used to follow the reaction in a spectral range between 340-1000 nm with a photodiode array detector. Under the experimental conditions employed, the instrument dead time was ~ 1.28 ms. Final FPR concentration was 7 μM, while nucleotide concentrations were 15, 150 and 300 μM. Multiple wavelength absorption data were collected and processed using the X-SCAN software (Applied Photophysics Ltd.). Typically, 400 spectra per second were collected. Experiments were carried out at 25 ºC in 50 mM Tris-HCl, pH 8.0. Photodiode array spectral deconvolution was performed by global analysis and numerical integration methods using the Pro-K software (Applied Photophysics Ltd.). Data collected over ranges from

1.28-200 ms were fit to a two-step, **A** > **B** > **C** model, allowing estimation of the conversion rate constants. The error in the estimated values was ± 15 %. Species **A**, **B** and **C** are spectral species, reflecting a distribution of enzyme intermediates at a certain point along the reaction time course, and do not necessarily represent a single distinct enzyme intermediate. Moreover, none of them represents individual species of products or reactants, and their spectra can not be included as fixed values in the global fitting. Model validity was assessed by lack of systematic deviations from residual plots at different wavelengths, inspection of calculated spectra and consistence among the number of significant singular values with the fitted model.

Spectra of the intermediate complexes CT-1 and CT-2 were estimated using the Pro-Kineticist II software (Applied Photophysics Ltd.), by analysis of the photodiode array data for the reaction of 6.4 μM FPR_{ox} with 150 μM NADPH under pseudo-first order conditions (Fig. 6(a)). The three-step mechanism FPR_{ox} + NADPH ⇔ CT-1 ⇔ CT-2 ⇔ FPR_{rd} + $NADP^+$ proposed for plastidic FNRs [28, 29] was used in combination with the spectra of free *R. capsulatus* FPR_{ox} and FPR_{rd} forms, the kinetic constants here derived and the interaction parameters previously reported for the complexes of FPR_{ox} with NADPH and $NADP^+$ [19]. Time-dependent spectral simulations were performed using the Pro-K software. During simulations, FPR_{ox} was considered to present a single absorbance maximum at 452 nm with a bandwidth of 17 nm and a relative height of 10.9 (extinction coefficient value), whereas FPR_{rd} was simulated by two absorbance maxima at 350 nm and 402 nm with bandwidths of 20 and 40 nm, and heights of 4.5 and 3.6, respectively. CT-1 was considered as displaying two absorbance maxima at 455 and 547 nm with bandwidths of 18 and 45 nm, and heights of 11.5 and 0.9, respectively. The corresponding parameters for CT-2 were: absorbance maxima at 474 and 856 nm, bandwidths of 38 and 140 nm and heights of 1.3 and 2.6, respectively.

Results

Interaction of R. capsulatus FPR with $NADP^+$ and analogues

Addition of nucleotides to oxidised chloroplast FNR (FNR_{ox}) leads to spectral changes in the visible region indicating perturbation of the FAD environment. The shapes of the difference spectra provide information on the relative arrangement of the ligand and the flavoenzyme upon complex formation. In the case of $NADP^+$, the appearance of a positive differential signal at 500-510 nm, resulting from a red shift of the peak corresponding to transition I of the flavin ring, has been associated with a stacking interaction of the nicotinamide with the isoaloxazine ring that correlates with efficient hydride transfer [29, 32], (see also Figure 1(a)). Nucleotide analogues that lack nicotinamide, such as 2'-P-AMP and 2'-P-ADP-ribose, elicit perturbations at shorter wavelengths [28, 44].

Difference spectra of bacterial-type reductases in complex with $NADP^+$ have not been reported so far. Figure 1(a) shows that *R. capsulatus* FPR displays spectral perturbations similar to those observed with chloroplast FNR when titrated until saturation with $NADP^+$, with a valley at 450 nm and peaks at 390 nm and 505 nm. To allow comparison with related enzymes, the normalised difference spectra of wild-type pea and *Anabaena* FNR_{ox}, as well as the pea Y308S mutant were included in Figure 1(a). The difference spectrum obtained with 2'-P-AMP was similar to those elicited by all members of the family, with a maximum at 460 nm and a valley at 405 nm (Figure 1(b)). Binding of NAD^+ was weaker and did not involve interaction with the flavin, as judged by the absence of the 505-nm peak (Figure 1(b)).

From this type of experiments, the affinities of the enzyme for $NADP^+$ and analogues could be determined (inset Figure 1b and Table 2). The K_d for $NADP^+$ was 222 ± 5 μM (Table 2), at least 20-fold higher than those reported for the plant and cyanobacterial reductases [28, 30. 32]. Moreover, a K_d of 204 ± 4 μM was also calculated for the interaction of 2'-P-AMP with *Rhodobacter* FPR (Table 2), suggesting that these interactions of the 2'-P-AMP moiety lead the docking of the NADP(H) molecule with the protein, as it was proposed for the *Anabaena* reductase [23]. Efforts were made then to determine the crystal structure of the *Rhodobacter* FPR-substrate complex to visualise the structural traits of nucleotide binding and affinity.

Three-dimensional structure of R. capsulatus FPR in complex with $NADP^+$ and 2'-P-AMP

Co-crystallisation protocols allowed us to obtain one single complex of *Rhodobacter* FPR with 2'-P-AMP and three different complexes with $NADP^+$, referred to as Forms I, II and III. Superposition of the crystallographic structures of the four complexes showed a conserved overall conformation of the protein, relative to the free enzyme [19] (PDB code 2bgi), yielding rmsd values of 0.3-0.7 Å for 255 Cα atoms. Although the higher rmsd numbers largely correspond to conformational variations alongside loops involved in crystalline packing contacts among the different crystallisation forms, the structural differences observed in the C-terminal tail (residues 266 to 272) appear to be related to the interaction of FPR with $NADP^+$ (see below).

In the four complexes obtained, the nucleotides bind exclusively through the adenosine moiety, which exhibits an excellent electron density map in all cases. Superposition of the resulting models indicates that the adenosine presents the same conformation and displays identical interactions with the FPR (Figures 2 a and b).

The adenosine moiety binds into a cavity formed by residues of four segments conserved in the FPR/FNR family: (1) the loop connecting β7-3_{10}2 (residues 128 to 130), (2) the β8-α4 loop (residues 158 to 163), (3) the β9-α6A loop including the α6A helix (residues 193 to 205), and (4) the β10-α7 loop and α7 helix (residues 233 to 240)(See figs. 2 a and b). The adenosine binding site is essentially formed by three arginines, R158, R195 and R203, which stabilise the nucleotide by interacting with its aromatic ring and the two phosphate groups (Figure 2b). The adenine ring is stabilised by a cation-π interaction established with the R203 side chain, by hydrophobic contacts with F237, and by three H-bonds formed by nitrogen atoms of the aromatic ring: directly with the D240 side chain, and through a water molecule with the T205 and S234 side chains and the I204 amide group (Figure 2b). On the other hand, the 5'-P interacts with R158, while the 2'-P is stabilised by contacts with R195 and R203. H-bond interactions also participate in the stabilisation of the phosphates. They are formed between the 2'-P group and the T194 side chain, and between the 5'-P group and G129 through a water molecule. Finally, the ribose ring contributes to stabilisation of the cofactor by an H-bond interaction between the O3 of the saccharide ring and the T194 side chain (Figure 2b).

The nicotinamide moiety shows remarkable conformational differences in the various $NADP^+$ complexes (Figure 2a). Models were obtained for the FPR-$NADP^+$ complexes I and II, (Figure 3) but no electron density was observed for the nicotinamide in the FPR-$NADP^+$ III complex, and this part of the molecule could not be modelled. In the three forms, the pyrophosphate group is stabilised by interactions with R158 and R195.

Interestingly enough, $NADP^+$ binding to FPR is accompanied by displacement of the C-terminal tail (residues 268-272), as well as by an increase of the B-factor values in this region with respect to the free enzyme (Table 3, Figure 4). Rmsd values for the Cα

atoms of the C-terminal region deviated from those of free FPR by 0.2-0.5 Å (Figure 4). In the case of the FPR-$NADP^+$ III complex, mobility was so high that residues 270-272 from monomers B and D could not be modelled due to their poor electron density (Figure 4). In contrast, the calculated rmsd deviations (0.1 Å) and the B-factor values for the FPR complex with 2'-P-AMP did not show significant variations when compared with the structure of the free reductase (Table 3, Figure 4).

Detailed analysis of the interactions established by the C-terminal region in the complexes relative to the free enzyme reveals two facts. First, the salt bridge between R158 and the C-terminal I272 described in free FPR [19] is maintained in complexes I and II, but is missing in monomers B and D of the FPR-$NADP^+$ III complex, where the three terminal residues 270-272 were not visible (Figure 5). Second, binding of $NADP^+$ or 2'-P-AMP is accompanied by formation of a new salt bridge between the guanidinum group of R158 and the carboxylic group of the E162 side chain (Figure 5). Moreover, the presence of the pyrophosphate (or 5'-P in the case of 2'-P-AMP) leads to displacement of the R158 side chain, which orients to stabilise the phosphates of the nucleotide and likely release a mobile C-terminus. This new conformation of R158 is accompanied by approximation to E162, allowing formation of the new salt bridge (Figure 5). At difference with both studies, binding equilibria analysis and X-ray crystallography, stopped-flow experiments reflect the interaction of the redox partners during hydride exchange.

Single turnover kinetics

Previously, single turnover reactions between *R. capsulatus* FPR and NADP(H) have been followed by single-wavelength stopped-flow methods at 452 nm, allowing only estimation of flavin reduction rates [19]. To identify possible intermediates in the reaction pathway absorbing at different wavelengths, we studied hydride transfer from

NADPH to *R. capsulatus* FPR_{ox} by stopped-flow anaerobic techniques using photodiode array detection and singular value deconvolution methods (Figures 6(a) and (b)). The first recorded spectrum after mixing FPR_{ox} with saturating concentrations of NADPH (1.28 ms, bold line in Figure 6(a)) showed the appearance of a long-wavelength absorbance band around 560 nm. This type of band has already been observed in the reactions of other flavoenzymes with pyridine nucleotides, being attributed to charge-transfer (CT) interactions between the oxidised isoalloxazine and the reduced nicotinamide, in our case FPR_{ox}-NADPH or CT-1 using previous terminologies [28, 29]. In this spectrum, the flavin absorbance band I (452 nm) only showed a slight decrease indicating that no hydride transfer takes place within this period, although CT-1 formation appears to be a relatively fast process. Spectra recorded at different times after the initial showed a decrease of flavin band I, indicating reduction, as well as the appearance of a second charge-transfer band centred around 850 nm and consistent with the formation of a FPR_{rd}-$NADP^+$ CT complex, CT-2 [28, 29]. Full FNR reduction was not achieved at equilibrium and the spectrum of the final mixture clearly revealed the presence of both CT-1 and CT-2, in contrast to the plastidic FNRs where CT-2 accumulated to a very small extent [29].

Spectra were recorded as a function of time and fitted globally by numerical integration. An **A** > **B** > **C** kinetic model was the most satisfactory in describing the absorbance changes. Figure 6(b) shows the species obtained by global analysis deconvolution of Figure 6(a) data. The first species observed after mixing, **A**, showed a spectrum consistent with FPR being present mainly in its oxidised state, but already showing the appearance of traces of a 500-600 broad band consistent with CT-1. Under saturating NADPH concentrations, **A** rapidly evolved to form species **B** with an observed rate constant (k_{obs1}) ≥ 350 s^{-1}. Comparison of **B** with **A** indicated accumulation of CT-1,

characterised by a band centred around 560 nm. Therefore, **B** appears to be mainly formed by CT-1. **B** further evolved to produce species **C** with a limit k_{obs2} = 160 s^{-1}. This process involved formation of the long broad band around 850 nm and an important decrease in the absorption intensity at 452 nm. Such changes in the spectra are consistent with hydride transfer and conversion of CT-1 into CT-2 in an equilibrium situation (species **C**) characterised by the presence of both CT bands. The observed rates are in excellent agreement with those obtained by Nogués *et al*. [19] using single-wavelength stopped-flow methods (150 s^{-1}). The simplest scheme accounting for the experimental results is:

$$\underbrace{FNR_{ox} + NADPH \Leftrightarrow [FNR_{ox}\text{-}NADPH]}_{\mathbf{A} > \mathbf{B}} \Leftrightarrow \underbrace{[FNR_{rd}\text{-}NADP^{+}] \Leftrightarrow FNR_{rd} + NADP^{+}}_{\mathbf{B} > \mathbf{C}}$$

Scheme 1

Spectra of the intermediate CT-1 and CT-2 species were estimated by analysis of the spectral data along time for the reaction of FPR_{ox} with NADPH under pseudo-first order conditions (Figure 6(a)), taking into account the three-step mechanism depicted in Scheme 1 and the kinetic constants derived from our deconvolution analysis. The spectrum derived for CT-1 displayed maxima at 455 nm and 547 nm, with extinction coefficients of 11.5 mM^{-1} cm^{-1} (slightly larger than that of free FPR_{ox}, 10.9 mM^{-1} cm^{-1}) and 0.9 mM^{-1} cm^{-1}, respectively, and a shoulder at 477 nm. CT-2 was characterised by maxima at 474 nm and 856 nm, with extinction coefficients of 1.3 mM^{-1} cm^{-1} and 2.6 mM^{-1} cm^{-1}, respectively (Figure 6(c)). The properties of the CT-1 and CT-2 spectra for *R. capsulatus* FPR were consistent with those of the equivalent complexes reported for

photosynthetic FNRs or phthalate dioxygenase reductase when reacting with NADPH and NADH, respectively [28, 29, 45].

A simulation analysis was carried out (Figure 6(c)) to validate the spectral positions and relative extinction coefficients derived for CT-1 and CT-2 species, the kinetic parameters resulting from the present study and the previously estimated k_{obs} obtained from single wavelength stopped/flow analysis [19]. Comparison of the resulting simulated spectra as a function of time and the evolution of the different species (Figure 6(d)) with the experimental data in Figure 6(a) indicated that our model reproduced the experimental observations. Comparison of simulated evolution of species and absorbance at 452 nm (inset in Figure 6(d)) with experimental absorbance changes at 452 nm (insets in Figure 6(a) and (b)) were also consistent with the assumption that some of the derived kinetic rate constants are just lower limit values, especially for CT-1 formation.

Discussion

Transition from slow-turnover bacterial-type FPR to highly active plastidic/cyanobacterial-type FNR involved major changes in FAD from a bent to an extended conformation, the gain of 30-50 amino acids and mutation of ~70 % of the remaining residues [5]. However, the individual step(s) – namely, substrate binding, product release, hydride and electron transfer, etc. – affected by the multiple modifications undergone by the enzyme remain(s) yet to be identified.

We describe herein the features of NADP(H) binding and hydride transfer by *R. capsulatus* FPR, which represents the reductive step in these bacterial-type reductases. This half-reaction has been thoroughly studied in the plant and *Anabaena* enzymes, and proposed to follow the mechanism [29] depicted in scheme 2:

Scheme 2

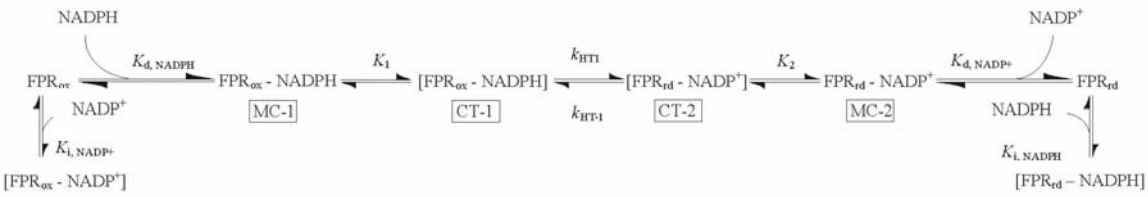

In which FPR_{ox}-NADPH and FPR_{rd}-$NADP^+$ are the Michaelis-Menten complexes MC-1 and MC-2, respectively, whereas [FPR_{ox}-NADPH] and [FPR_{rd}-$NADP^+$] are the charge-transfer complexes CT-1 and CT-2, respectively. Results included in Figures 1 and 6 indicate that reaction of *R. capsulatus* FPR with NADP(H) proceeds essentially through the same general mechanism, and binding and kinetic parameters for most of the individual steps could be estimated (Table 2), allowing side-by-side comparison with those previously determined for the plastid-type reductases [28, 29, 32, 46].

The nicotinamide and isoalloxazine ring systems form an angle of ~ 30° in binary complexes of NADP(H) with pea and *Anabaena* FNRs [11, 34]. This interaction is likely responsible for the red shift of flavin transition I and the appearance of the positive peak at 500-510 nm in difference spectra [32]. Figure 1 shows that addition of $NADP^+$ to *R. capsulatus* FPR_{ox} elicits a similar perturbation, suggesting that the main features of nicotinamide docking were not significantly altered during the transition to the plastidic-class reductases. As already indicated, displacement of the C-terminal tyrosine in this class of FNRs is required to allow productive accommodation of the nicotinamide and, accordingly, substitution of this residue by a serine (Y308S and Y303S mutants of pea and *Anabaena* FNR, respectively) leads to a dramatic increase in the intensity of the 510 nm difference peak [32, 34]. Then, the magnitude of this absorption maximum provides an estimation of the degree of nicotinamide occupancy in the equilibrium, assuming that the Y-to-S C-terminal mutant represents 100 % stacking

[32]. This value, which gives a rough estimation of the difficulties to form the catalytic complex, varies widely even among plastidic-class reductases. Chloroplast FNR displays ~ 15 % nicotinamide occupancy in the equilibrium, but the enzymes from cyanobacteria (Figure 1(a)) and heterotrophic plastids [47] exhibit only marginal perturbations in this region. The amplitude of the 505 nm peak in the *Rhodobacter* enzyme was ~ 10 % of the one obtained with the Y308S mutant FNR, a value close to that of the wild-type pea enzyme (Figure 1(a), inset). The results thus indicate that the nicotinamide of $NADP^+$ has access to the isoalloxazine moiety in the soluble binary complex of *R. capsulatus* FPR. It is thus conceivable, that the C-terminal tail could modulate NMN occupancy in the catalytic cavity of FPR, as done by the C-terminal tyrosine in FNRs.

A note of caution should be introduced when interpreting these results, since the FPR_{ox}-$NADP^+$ complex is not an intermediate of the reaction mechanism. Rather, $NADP^+$ behaves as a competitive inhibitor with respect to NADPH in the extreme left of Scheme 2. However, Deng *et al*. [11] have shown that the docking mode of the bound nucleotide does not change significantly upon reduction, indicating that the conformation of the FPR_{ox}-$NADP^+$ complex truly reflects those of all intermediate complexes in Scheme 2. A close interaction between the nicotinamide and the isoalloxazine was also indicated by formation of the charge-transfer complexes CT-1 and CT-2 (Figure 6). CT interactions between these cofactors are not an absolute requirement for efficient hydride transfer in all flavoenzymes [48], but an excellent correlation between CT complex formation and catalysis has been demonstrated for FNR [28]. Hydride transfer takes place in a narrow cleft of the active site in this type of reductases, and the nicotinamide needs to slide over the isoalloxazine ring system to approach the reacting N-5 atom of the flavin [11].

Dissociation constants for $NADP^+$ and NADPH binding to *R. capsulatus* FPR, as determined by differential spectroscopy (Figure 1) and stopped-flow procedures (Figure 6), respectively, were about 20-fold higher than those obtained for their plastid-type counterparts (Table 2). Kinetic parameters for CT formation and interconversion (hydride transfer) were instead lower (Table 2). The comparatively low velocities with respect to plastid-type enzymes indicate that formation of the productive complexes is less favoured, but CT formation also suggests that orientation for efficient hydride transfer is properly achieved in the bacterial FPRs. Then, although NADP(H) is able to stabilise a catalytically productive conformation when bound to the *Rhodobacter* enzyme, as reflected by CTs and binding equilibria spectra, the sole stacking geometry between nicotinamide and isoaloxazine rings does not assure a fast hydride transfer and reduction of the FPR.

Spectroscopic and structural analysis of $NADP^+$ binding to plastidic-class FNRs have shown that the strength of nucleotide attachment is largely determined by interactions of the enzyme with the 2'-P-AMP moiety and the pyrophosphate bridge [8, 23, 34], whereas the NMN portion weakened rather than stabilised the interaction [11, 28, 32]. Accordingly, only the 2'-P-AMP region docked properly in crystals of wild-type FNR in complex with $NADP^+$, and even when the NMN moiety could be modelled in some cases, it always pointed to solvent, too far away from the flavin site to represent a meaningful conformation for hydride transfer [10, 23]. We therefore analysed the ability of *R. capsulatus* FPR to bind 2'-P-AMP in solution (Figure 1(b)), and the crystal structure of the enzyme in complex with both 2'-P-AMP and $NADP^+$ (Figures 2-5).

As anticipated, interaction with 2'-P-AMP was relatively weak, with K_d values that were about 100-fold higher than those reported for plastidic-class FNRs (Table 2). As in the latter group of reductases, crystalline complexes with both 2'-P-AMP and $NADP^+$

only displayed a good electron density for the bound 2'-P-AMP moiety and a disordered NMN, sometimes stabilised by non-specific contacts with the protein (Figures 2-5). When the structures of these FPR complexes were superimposed to similar ones obtained for the plastidic-class FNRs, the adenosine binding region of FPR appears displaced ~ 2.5 Å due to changes in the α7 and α6A helices and the β9-α6A and β10-α7 loops (see Figure 7). In addition to these local displacements, the presence of the C-terminal tail in FPR generates a narrower adenosine binding cavity respect to that found in plastidic-class FNRs, which may difficult coenzyme binding through the 2'-P-AMP moiety at initial steps. On nucleotide association, *R. capsulatus* FPR does not undergo the reorganisation of the region involved in pyrophosphate recognition that is typical of NADP(H)-dependent members of the larger FNR structural family. This outcome had been already inferred by inspection of the free enzyme structure [19]. In this sense, FPR behaves more like the NAD(H)-dependent enzymes of the family.

Nucleotide binding leads to displacement of the C-terminal region of the protein (Figure 5), indicating that this sub-domain has a more dynamic conformation than the rest of the protein. It is tempting to speculate that the whole C-terminal loop of *R. capsulatus* FPR moves away during turnover to accommodate the nicotinamide and flavin rings for hydride transfer, supporting a dynamic picture of the reaction. Moreover, crystallographic complexes reveal that R158 could play a pivotal role in this movement. In the native state, R158 is involved in a salt bridge interaction with the carboxylate of I272, the last FPR residue, therefore stabilising the C-terminal tail and "closing" the NADP(H) binding site. Upon $NADP^+$ binding, R158 changes orientation and forms a new salt bridge interaction (R158-E162) which stabilises the pyrophosphate moiety of the coenzyme and could facilitate rearrangement of the C-terminal tail. Besides, comparison of FPR structures from *R. capsulatus* with functional complexes obtained

with pea and *Anabaena* FNR mutants suggest that, during displacement of the C-terminal region, the adenosine of FAD could also suffer a conformational change in order to accommodate the nicotinamide. NADPH oxidation by *Rhodobacter* FPR without displacement of the C-terminal tail, including Ala266 facing the isoaloxazine ring, would imply electron tunneling from the nicotinamide through amino acid residues, and the generation of a cation radical form of the coenzyme. To the best of our knowledge, such intermediate species during multistep hydride transfer have only been described in the case of NAD(P)H functioning as monoelectronic quencher of catalase compounds I and II [49] or in models for photochemical/thermal non-enzymatic oxidation of dihydropiridines [50, 51]. A recent structural study on the *Pseudomonas aeruginosa* FPR, suggested that bacterial-class reductases might be reduced by NADPH following a stepwise electron-proton-electron transfer mechanism, although no experimental data supporting this hypothesis was provided [53]. Fast kinetic measurements of *Rhodobacter* FPR reduction by NADPH reveal the occurrence of two charge transfer bands along the reaction, corresponding to the CT-1 and CT-2 complexes described previously for plastidic FNRs. These data suggest that the reaction occurs through a hydride transfer mechanism for both, plastidic and bacterial-class reductases, and a stepwise electron-proton-electron transfer mechanism should be discarded, at least in the *R. capsulatus* enzyme.

The similarities between FPR and FNR discussed above might be deceiving, however, since the composition and distribution of the protein residues that stabilise the coenzyme are fairly different in *R. capsulatus* reductase. Three arginines are involved in 2'-P-AMP recognition, R158, R195 and R203, but only R195 is conserved, in sequence, *locus* and function, in plastidic-class reductases. R158 participates in stabilisation of the 5'-P group and is absent in FNRs, being replaced by a proline (P194 in *Anabaena*

FNR). It may be involved in pyrophosphate recognition instead of the highly conserved arginine/lysine residue found in plastidic-class enzymes [23] (R100 in *Anabaena* FNR) (Figure 7).

A remarkable difference between the two types of reductases concerns R203, which plays a double role in *Rhodobacter* FPR, interacting with the 2'-P group and the adenosine ring. In *Anabaena* FNR, stabilisation of the 2'-P involves salt bridges with R224 and R233 which belong to the same loop that R203 in FPR and are conserved in plastidic-class FNRs as lysine or arginine. There is a labour division with respect to adenosine stabilisation in this class of enzymes, where a conserved tyrosine (Y235 in *Anabaena* FNR) [23] occupies the position of R203 [19], displaying a π-π interaction with the adenosine instead of the cation-π interaction of *R. capsulatus* FPR (Figure 7). The effects of this change on nucleotide affinity are unknown, but replacement of Y235 in *Anabaena* FNR by an alanine residue led to a mutant enzyme with decreased hydride transfer rates and lower affinity for NADP(H), displaying kinetic parameters similar to those of wild-type bacterial FPRs [29]. Moreover, the three arginines involved in adenosine binding in *Rhodobacter* FPR are strictly conserved in the structures of the other bacterial reductases reported, those from *E. coli*, *Azotobacter vinelandii* and *Pseudomonas aeruginosa* [17, 18, 21]. In *E. coli* FPR, the roles of these three arginines have been already tested by site-directed mutagenesis experiments [52]. Mutation of each of these arginines by alanine generated remarkable changes in the catalytic efficiency as well as in the ability for discriminating between NADP(H) an NAD(H). The results reflect the importance of these residues in coenzyme recognition and discrimination. Interestingly, the most drastic effect was observed in the R184A mutant (equivalent to R203 in *Rhodobacter* FPR) which displayed a decreased catalytic efficiency and an inversion in NADP(H)/NAD(H) discrimination respect to the wild-

type enzyme [52]. All these observations support the notion that FPRs display a different mechanism for coenzyme recognition relative to their plastidic-class homologues.

For the plastidic enzyme, a sequential ordered mechanism has been proposed being $NADP^+$ the leader substrate, and including the ternary complex as required intermediate [46]. Batie and Kamin confirmed that binding of $NADP^+$ increases the rate of FNR reduction in the ternary complex by facilitating dissociation of oxidised Fd, which suggests a global influence of the nucleotide binding on the enzyme structure [46]. However, the structures of the crystalised FNR:$NADP^+$ binary complexes from *Anabaena* and pea, display an overall structure equivalent to the unbound native enzyme, with no significant changes in the relative orientation of the FAD and $NADP^+$ binding domains [11, 23]. On the other side, notable structural perturbations were described for the plastidic reductase complexed with Fd [12]. Upon complex formation, the relative position of the whole $NADP^+$ domain changes slightly as a single unit, but the most remarkable difference resides at the conserved Glu 312, which moves towards the conserved Ser 96 into hydrogen bonding distance, probably optimising the geometry of the $NADP^+$ molecule for a productive interaction with FAD [12]. In view of these results, a possible influence of the proteic substrate of *Rhodobacter* FPR on the affinity of $NADP^+$, the mode of binding and the rates of hydride transfer reported here should not be disregarded.

In conclussion, we propose that transition from eubacterial FPR to cyanobacterial FNR involved several structural changes:

1) the accessibility of the adenosine binding site, which is decreased respect to plastidic-class reductases,

2) bacterial-class reductases contain three arginines at the adenosine binding site, two of them (R158 and R203) not conserved in the plastidic-class FNRs. In this sense, the adenosine-interacting arginine (R203) found in FPRs is substituted by a tyrosine in plastidic-class FNRs and it should be very interesting to learn if any activity advantage could be gained by replacing R203 of *R. capsulatus* FPR by a tyrosine. Respect to R158, it not only participates in stabilisation of the C-terminal region but also seems to play a key role in stabilisation of the NADP(H) pyrophosphate. These interactions differ from those observed in plastidic-class FNRs,

3) the C-terminal tail present in *R. capsulatus* FPR may displace to allow entrance of the NMN in the catalytic cavity and in addition, this movement could modulate nicotinamide occupancy, analogously to the C-terminal tyrosine found in plastidic-class enzymes. Experiments are currently underway to evaluate these hypotheses.

Aknowledgments: This work was supported by CONICET (PIP 5124) and ANPCyT (PICT 01-14648) from Argentina; and by Dirección General de Investigación (BFU2005-01645 and CSD 2006-00015) and Ministerio de Educación y Ciencia (BIO2007-65890-C02-01 to M. M.) from Spain. I. P.-D. is a fellow of CSIC (Spain). A. B. is a fellow of CONICET (Argentina) and N. Carrillo and N. Cortez are staff members of the same Institution.

References

1. J.K. Hurley, R. Morales, M. Martínez-Júlvez, T.B. Brodie, M. Medina, C. Gómez-Moreno, G. Tollin, Structure–function relationships in *Anabaena* ferredoxin/ferredoxin:$NADP^+$ reductase electron transfer: insights from site-directed mutagenesis, transient absorption spectroscopy and X-ray crystallography, Biochim. Biophys. Acta 1554 (2002) 5-21.

2. N. Carrillo, E.A. Ceccarelli, Open questions in ferredoxin-NADP(H) reductase catalytic mechanism, Eur. J. Biochem. 270 (2003) 1900-1915.

3. M. Medina, C. Gómez-Moreno, Interaction of ferredoxin–$NADP^+$ reductase with its substrates: optimal interaction for efficient electron transfer, Photosynth. Res. 79 (2004) 113-131.

4. P. A. Karplus, H.R. Faber, Structural aspects of plant ferredoxin:$NADP^+$ oxidoreductases, Photosynth. Res. 81 (2004) 303-315.

5. E.A. Ceccarelli, A.K. Arakaki, N. Cortez, N. Carrillo, Functional plasticity and catalytic efficiency in plant and bacterial ferredoxin-NADP(H) reductases, Biochim. Biophys. Acta 1698 (2004) 155-165.

6. G.T. Hanke, G. Kurisu, M. Kusunoki, T. Hase, Fd:FNR electron transfer complexes: evolutionary refinement of structural interactions, Photosynth. Res. 81 (2004) 17-327.

7. M. Medina, A. Luquita, J. Tejero, J.A. Hermoso, T. Mayoral, J. Sanz-Aparicio, K. Grever, C. Gómez-Moreno, Probing the determinants of coenzyme specificity in ferredoxin-$NADP^+$ reductase by site-directed mutagenesis, J. Biol. Chem. 276 (2001) 11902-11912.

8. J. Tejero,M. Martínez-Júlvez, T. Mayoral, A. Luquita, J. Sanz-Aparicio, J.A. Hermoso, J.K. Hurley, G. Tollin, C. Gómez-Moreno, M. Medina, Involvement of the pyrophosphate and the 2'-phosphate binding regions of ferredoxin-$NADP^+$ reductase in coenzyme specificity, J. Biol. Chem. 278 (2003) 49203-49214.

9. P.A. Karplus, M.J. Daniels, J.R. Herriott, Atomic structure of ferredoxin-$NADP^+$ reductase: prototype for a structurally novel flavoenzyme family, Science 251 (1991) 60-66.

10. C.M. Bruns, P.A. Karplus, Refined crystal structure of spinach ferredoxin-$NADP^+$ oxidoreductase at 1.7 Å resolution: oxidized, reduced and 2'-phospho-5'-AMP bound states, J. Mol. Biol. 247 (1995) 125-145.

11. Z. Deng, A. Aliverti, G. Zanetti, A.K. Arakaki, J. Ottado, E.G. Orellano, N.B. Calcaterra, E.A. Ceccarelli, N. Carrillo, P.A. Karplus, A productive $NADP^+$ binding mode of ferredoxin-$NADP^+$ reductase revealed by protein engineering and crystallographic studies, Nature Struct. Biol. 6 (1999) 847-853.

12. G. Kurisu, M. Kusunoki, E. Katoh, T. Yamazaki, K. Teshima, Y. Onda, Y. Kimata-Ariga, T. Hase, Structure of the electron transfer complex between ferredoxin and ferredoxin-$NADP^+$ reductase, Nature Struct. Biol. 8 (2001) 117-121.

13. A. Dorowski, A. Hofmann, C. Steegborn, M. Boicu, R. Huber, Crystal structure of paprika ferredoxin-$NADP^+$ reductase. Implications for the electron transfer pathway. J. Biol. Chem. 276 (2001) 9253-9263.

14. A. Aliverti, R. Faber, C.M. Finnerty, C. Ferioli, V. Pandini, A. Negri, P.A. Karplus, G. Zanetti, Biochemical and crystallographic characterization of ferredoxin-$NADP^+$ reductase from nonphotosynthetic tissues. Biochemistry 40 (2001) 14501-14508.

15. Y.H. Lee, K. Tamura, M. Maeda, M. Hocino, K. Sakurai, S. Takahashi, T. Ikegami, T. Hase, Y. Goto, Cores and pH-dependent dynamics of ferredoxin-$NADP^+$ reductase revealed by hydrogen/deuterium exchange, J. Biol. Chem. 282 (2007) 5959-5967.

16. L. Serre, F.M. Vellieux, M., Medina, C. Gómez-Moreno, J.C.Fontecilla-Camps, M. Frey, X-ray structure of the ferredoxin-$NADP^+$ reductase from the cyanobacterium *Anabaena* PCC7119 at 1.8 Å resolution, and crystallographic studies of $NADP^+$ binding at 2.25 Å resolution. J. Mol. Biol. 263 (1996) 20-39.

17. M. Ingelman, V. Bianchi, H. Eklund, The three-dimensional structure of flavodoxin reductase from *Escherichia coli* at 1.7 Å resolution, J. Mol. Biol. 268 (1997) 147-157.

18. G. Sridhar Prasad, N. Kresge, A.B. Muhlberg, A. Shaw, Y.S. Jung, B.K. Burgess, C.D. Stout, The crystal structure of NADPH:ferredoxin reductase from *Azotobacter vinelandii*, Protein Sci. 7 (1998) 2541-2549.

19. I. Nogués, I. Pérez-Dorado, S. Frago, C. Bittel, S.G. Mayhew, C. Gómez-Moreno, J.A. Hermoso, M. Medina, N. Cortez, N. Carrillo, The ferredoxin-NADP(H) reductase from *Rhodobacter capsulatus*: molecular structure and catalytic mechanism, Biochemistry 44 (2005) 11730-11740.

20. A.S. Nascimento, D.L. Catalano-Dupuy, A. Bernardes, M. de Oliveira Neto, M.A. Santos, E.A. Cecarelli, I. Polikarpov, Crystal structures of *Leptospira interrogans* FAD-contining ferredoxin $NADP^+$ reductase and its complex with $NADP^+$. BMC Struct. Biol. 7 (2007) 69.

21. A. Wang, Y. Zeng, H. Han, S. Weeratunga, B.N. Morgan, P. Moënne-Loccoz, E. Schönnbrunn, M. Rivera, Biochemical and structural characterization of *Pseudomonas aeruginosa* Bfd and FPR: ferredoxin-$NADP^+$ reductase and not ferredoxin is the redox

partner of heme oxygenase under iron-starvation conditions, Biochemistry 46 (2007) 12198-12211.

22. M. Milani, E. Balconi, A. Aliverti, E. Mastrangelo, F. Seeber, M. Bolognesi, G. Zanetti, Ferredoxin-NADP+ reductase from *Plasmodium falciparum* undergoes NADP+-dependent dimerization and inactivation: functional and crystallographic analysis. J. Mol. Biol. 367 (2007) 501-513

23. J.A. Hermoso, T. Mayoral, M. Faro, C. Gómez-Moreno, J. Sanz-Aparicio, M. Medina, Mechanism of coenzyme recognition and binding revealed by crystal structure analysis of ferredoxin-$NADP^+$ reductase complexed with $NADP^+$, J. Mol. Biol. 319 (2002) 1133-1142.

24. I.F. Sevrioukova, H. Li, T.L. Poulos, Crystal structure of putidaredoxin reductase from *Pseudomonas putida*, the final structural component of the cytochrome P450cam monooxygenase, J. Mol. Biol. 336 (2004) 889-902.

25. D. Seo, K. Kamino, K. Inoue, H. Sakurai, Purification and characterization of ferredoxin-$NADP^+$ reductase encoded by *Bacillus subtilis yumC*, Arch. Microbiol. 182 (2004) 80-89.

26. C.C. Correll, M.L. Ludwig, C.M. Bruns, P.A. Karplus, Structural prototypes for an extended family of flavoprotein reductases. Comparison of phthalate dioxygenase reductase with ferredoxin reductase and ferredoxin, Protein Sci. 2 (1993) 2112-2133.

27. M. Ingelman, S. Ramaswamy, V. Nivière, M. Fontecave, H. Eklund, Crystal structure of NAD(P)H:flavin oxidoreductase from *Escherichia coli*, Biochemistry 38 (1999) 7040-7049.

28. C.J. Batie, H. Kamin, Association of ferredoxin-$NADP^+$ reductase with NADP(H). Specificity and oxidation-reduction properties, J. Biol. Chem. 261 (1986) 11214-11223.

29. J. Tejero, J.R. Peregrina, M. Martínez-Júlvez, A. Gutiérrez, N.S. Scrutton, C. Gómez-Moreno, M. Medina, Catalytic mechanism of the hydride transfer between $NADP^+$/H and ferredoxin-$NADP^+$ reductase from *Anabaena* PCC7119, Arch. Biochem. Biophys. (2007) 459, 79-90.

30. M. Medina, M. Martínez-Júlvez, J.K. Hurley, G. Tollin, C. Gómez-Moreno, Involvement of glutamic acid 301 in the catalytic mechanism of ferredoxin-$NADP^+$ reductase from *Anabaena* PCC 7119, Biochemistry 37 (1998) 2715-2728

31. C. Bittel, L.C. Tabares, M. Armesto, N. Carrillo, N. Cortez, The oxidant-responsive diaphorase of *Rhodobacter capsulatus* is a ferredoxin(flavodoxin)-NADP(H) reductase, FEBS Lett. 553 (2003) 408-412.

32. L. Piubelli, A. Aliverti, A.K. Arakaki, N. Carrillo, E.A. Ceccarelli, P.A. Karplus, G. Zanetti, Competition between C-terminal tyrosine and nicotinamide modulates pyridine nucleotide affinity and specificity in plant ferredoxin-$NADP^+$ reductase, J. Biol. Chem. 275 (2000) 10472-10476.

33. I. Nogués, J. Tejero, J.K. Hurley, D. Paladini, S. Frago, G. Tollin, S.G. Mayhew, C. Gómez-Moreno, E.A. Ceccarelli, N. Carrillo, M. Medina, Role of the tyrosine of ferredoxin-nicotinamide adenine dinucleotide phosphate reductase in the electron transfer processes with its protein partners ferredoxin and flavodoxin, Biochemistry 43 (2004) 6127-6137.

34. J. Tejero, I. Pérez-Dorado, C. Maya, M. Martínez-Júlvez, J. Sanz-Aparicio, C. Gómez-Moreno, J.A. Hermoso, M. Medina, C-terminal tyrosine of ferredoxin-$NADP^+$ reductase in the hydride transfer processes with $NAD(P)^+$/H, Biochemistry 44 (2005) 13477-13490.

35. N.B. Calcaterra, G.A. Picó, E.G. Orellano, J. Ottado, N. Carrillo, E.A. Ceccarelli, Contribution of the FAD binding site residue tyrosine 308 to the stability of pea ferredoxin-$NADP^+$ oxidoreductase, Biochemistry 34 (1995) 12842-12848.

36. A.G.W. Leslie, MOSFLM, in: J.R. Machin, Papiz, M. Z. (Eds.) *Proceedings of the CCP4 Study Weekend* Warrington, (1987), pp. 39-50, Warrington: SERC Daresbury Laboratory.

37. S. Bailey, The CCP4 suite, programs for protein crystallography, Acta Crystallogr. D 50 (1994) 760-763.

38. A. Vagin, A. Teplyakov, MOLREP, an automated program for molecular replacement, J. Appl. Cryst. 30 (1997) 1022-1025.

39. A.T. Brunger, P.D. Adams, G.M. Clore, W.L. DeLano, P. Gros, R.W. Grosse-Kunstleve, J.S. Jiang, J. Kuszewski, M. Nilges, N.S. Pannu, R.J. Read, L.M. Rice, T. Simonson, G.L. Warren Crystallography and NMR System, Acta Crystallogr. D 54 (1998) 905-921.

40. T.A. Jones, J.Y. Zou, S.W. Cowan, M. Kjeldgaard, Improved methods for model building in electron density maps and the location of errors in these models, Acta Crystallogr. A 47 (1991) 110-119.

41. R.A. Laskowski , M.W. MacArthur, D.S Moss,. J.M. Thornton, PROCHECK: a program to check the stereochemical quality of protein structures, J. Appl. Crystallogr. 26 (1993) 283-291.

42. R.W. Hooft, G. Vriend, C. Sander, E.E. Abola Errors in protein structures, Nature 38 (1996).272.

43. W.L. DeLano, The PyMol Molecular Graphics System, version 0.99, DeLano Scientific, San Carlos, CA, USA, http://www.pymol.org.

44. J. Sancho, C. Gómez-Moreno, Interaction of ferredoxin-$NADP^+$ reductase from *Anabaena* with its substrates, Arch. Biochem. Biophys. 288 (1991) 231-238.

45. G.T. Gassner, D.P. Ballou, Preparation and characterization of a truncated form of phthalate dioxygenase reductase that lacks an iron-sulfur domain. Biochemistry 34 (1995) 13460-13471.

46. C.J. Batie, H. Kamin, Electron transfer by ferredoxin-$NADP^+$ reductase. Rapid-reaction evidence for participation of a ternary complex, J. Biol. Chem. 259 (1984) 11976-11985.

47. A. Aliverti, V.Pandini, G. Zanetti, Domain exchange between isoforms of ferredoxin-$NADP^+$ reductase produces a functional enzyme, Biochim. Biophys. Acta 1696 (2004) 93-101.

48. M. Ortiz-Maldonado, B. Entsch, D.P. Ballou, Conformational changes combined with charge-transfer interactions are essential for reduction in catalysis by p-hydroxybenzoate hydroxylase. Biochemistry 42 (2003) 11234-11242.

49. Ö. Almarsson, A. Sinha, E. Gopinath, T.C. Bruice, Mechanism of one-electron oxidation of NAD(P)H and function of NADPH bound to catalase, J. Am. Chem. Soc. 115 (1993) 7093-7102.

50. A. Marcinek, J. Adamus, K. Huben, J. Gebicki, T.J. Bartczek, P. Bednarek, T. Ball, Hydrogen-transferred radical cations of NADH model compounds. 1. Spontaneous tautomerization, J. Am. Chem. Soc. 122 (2000) 437-443.

51. J. Zielonka, A. Marcinek, J. Adamjus, J. Gebicki, Direct observation of NADH radical cation generated in reactions with one-electron oxidants, J. Phys. Chem. A 17 (2003) 9860-9864.

52. C. Leadbeater, L. McIver, D. J. Campopiano, S.P. Webster, R.L. Baxter, S.S. Kelly, N.C. Price, D.A. Lysek, M.A. Noble, S.K. Chapman, A. Munro, Probing the NADPH-binding site of *Escherichia coli* flavodoxin oxidoreductase. Biochem. J. 352 (2000) 257-266.

53. A. Wang, J.C. Rodríguez, H. Hang, E. Shönbrunn, M. Rivera, X-ray crystalographic and solution state nuclear magnetic resonance spectroscopic investigations of $NADP^+$ binding to ferredoxin NADP reductase from Pseudomonas aeruginosa. Biochemistry 47 (2008) 8080-8093.

54. A.K. Arakaki, Participación de residuos aromáticos en la estructura y función de flavoproteínas, Ph D Thesis (2000) Universidad Nacional de Rosario.

Legends to Figures

Figure 1. Difference absorption spectra elicited by nucleotide binding to FPR and FNR. (a) Spectroscopic characterisation of the complexes between $NADP^+$ and *R. capsulatus* FPR (thick line), pea FNR (thin line) and *Anabaena* FNR (dotted line). The inset shows, in different absorbance scale, the comparison with the Y308S pea FNR mutant (dotted and long dash) between 475-550 nm. (b) Spectroscopic characterisation of the *R. capsulatus* FPR complexes with $NADP^+$ (thick line); NAD^+ (dotted line) and 2'-P-AMP (thin line). FPR spectra were recorded at 25 ºC under the conditions described in Materials and Methods. Those of the various FNRs were adapted from Piubelli *et al.* [32] and Medina *et al.* [7] The inset shows the maximum of absorbance as a function of $NADP^+$ (squares) or 2'-P-AMP (circles) concentration. Experimental data were fit to the rectangular hyperbola equation and the Kd was estimated.

Figure 2. Conformation of nucleotides bound to *R. capsulatus* FPR. (a) Stereoview representation of the superposition of the FPR complexes with $NADP^+$/2'-P-AMP and the free FPR. In the four FPR complexes, the nucleotide molecule binds the reductase through the adenosine moiety. Conformational changes from the Cα carbon representation of the C-terminal tail (Ct) are shown, which appears coloured in green (2'-P-AMP complex), magenta ($NADP^+$ complex, Form I), yellow ($NADP^+$ complex, Form II), blue ($NADP^+$ complex, Form III) and orange (free FPR). Cartoon in grey corresponds to the free FPR structure (except for the C-terminal tail). FAD and $NADP^+$/2'-P-AMP molecules are represented in sticks and they exhibit the same colour code followed with the C-terminal tail. Loops involved in coenzyme interaction are labelled. (b) Stereoview showing the interactions involved in adenosine moiety stabilisation (only those corresponding to the 2'-P-AMP complex are illustrated). The

2'-P-AMP molecule (in green), as well as those amino acids involved in cofactor stabilisation are represented in sticks (FPR is in orange).

Figure 3. Electron density map corresponding to the $NADP^+$ molecule in complex with *R. capsulatus* FPR. Electron density of the nucleotide molecule is shown in grey, FPR is in orange and $NADP^+$ molecules are in magenta (Form I), yellow (Form II) and cyan (Form III). The three arginines of the adenosine binding site are represented in orange sticks.

Figure 4. Comparison of the B-factor values in the FPR molecule shows significant mobility of the C-terminal tail associated with $NADP^+$ binding. B-factor values are represented in colour grades from blue (lower B-factor values) to red (higher B-factor values). Mobility of the polypeptide chain is also indicated by the width of the Cα chain which thickens as the B-factor value increases. FAD, $NADP^+$ and 2'-P-AMP are represented as black thin sticks and the C-terminal tail (Ct) is signposted by a black arrow.

Figure 5. Salt bridges involved in C-terminal tail stabilisation and coenzyme binding to *R. capsulatus* FPR. A salt bridge is formed in FPR between R158 and the carboxylic group of I272, an interaction that participates in stabilisation of the C-terminal tail conformation in the free enzyme. In the complexes with 2'-P-AMP and $NADP^+$, R158 moves toward E162 forming a different salt bridge which contributes to stabilisation of the pyrophosphate of $NADP^+$.

Figure 6. Evolution of spectral changes during reaction of oxidised *R. capsulatus* FPR with NADPH. (a) Time course of the reaction between 6.4 μM FPR_{ox} and 150 μM NADPH. Spectra were recorded every 2.56 ms. The corresponding protein spectrum before mixing is shown as a dotted line, and the first spectrum after mixing as a bold

line. Arrows indicate the direction of absorbance changes expressed in arbitrary units (A.U.). Spectra after mixing are shown at 1.28, 9.3, 11.9, 14.4, 17.0, 19.6, 22.1, 24.7, 29.8, 40.0 and 45.0 ms. The inset shows the absorption kinetic experimental transients obtained at 452 nm (line), 580 nm (open circles) and 840 nm (filled circles). The assay was carried out in 50 mM Tris-HCl, pH 8.0 and 25 ºC. (b) Absorbance spectra for the three pre-steady-state kinetically distinguishable species obtained by global analysis of the reaction in panel (a). Species are denoted as a bold line for the initial species **A**, a thin line for the intermediate species **B** and a dashed line for the final species **C**. The inset shows the corresponding evolution of species along time. (c) Spectra of CT intermediates derived by global analysis of the reaction of FPR_{ox} with NADPH; CT-1 (thin line) and CT-2 (dotted line). (d) Simulation of the evolution of the reaction of FPR_{ox} (6.4 μM) with NADPH (150 μM). Spectra simulated at 0.0, 0.5, 1.0, 1.5, 3.0, 4.5, 7.5, 13.5, 19.5, 25.5, 31.5, 37.5 and 49.5 ms. The inset shows evolution along time of the absorbance at 452 nm (bold line), 500 nm (thin line) and 856 nm (dotted line). A vertical dashed line indicates the part of the simulated process that must occur within the instrumental dead time (left) and the part experimentally observed (right).

Figure 7. Displacement of the 2'-P-AMP binding site in *R. capsulatus* FPR relative to plastidic-class FNRs. Superposition of the complex of *R. capsulatus* FPR (cartoon in orange) with 2'-P-AMP (green sticks), the complex of the Y303S mutant of *Anabaena* FNR (cartoon in blue) with $NADP^+$ (purple sticks) and the complex of wild-type *Anabaena* FNR with $NADP^+$ obtained by co-crystallization ($NADP^+$ as yellow sticks). Amino acids involved in cofactor stabilisation are represented in sticks. Those secondary structure elements of the *Rhodobacter* enzyme which differ from plastidic-class FNRs are labelled.

Table 1. Structure determination and statistics obtained for the complexes of *R. capsulatus* FPR with $NADP^+$ and 2'-P-AMP.

Ligand	$NADP^+$			2'-P-AMP
	Form I	Form II	Form III	
		Data collection statistics		
Space Group	$P3_121$	$P3_121$	$P2_1$	$P3_121$
Unit cell parameters				
a, Å	68.72	61.92	69.38	121.1
b, Å	68.72	61.92	93.45	121.1
c, Å	128.15	123.0	104.94	50.6
α, º	90.00	90.00	90.00	90.0
β, º	90.00	90.00	89.97	90.0
γ, º	120.00	120.00	90.00	120.0
No. of molecules/ua	1	1	4	1
X-ray source	Rotating anode	Synchrotron radiation (ID14-4,ESRF)	Synchrotron radiation (ID14-2, ESRF)	Synchrotron radiation (ID14-2, ESRF)
Wavelength, Å	1.5418	0.9786	0.9330	0.9330
Resolution, Å	30.28-2.13 (2.26-2.13)	53.63-2.27 (2.48-2.27)	49.21-1.93 (2.12 -1.93)	45.56-2.37 (2.73-2.37)
Total no. of reflections	139884	165639	406455	230081
No of unique reflections	43856	19685	122712	24368
Solvent (%)	57.8	45.8	56.6	65.5
Redundancy	3.2 (2.9)	7.5 (9.2)	3.4 (3.3)	5.9 (5.3)
Completeness (%)	99.4 (98.1)	99.8 (100)	94.6 (89.0)	98.9 (97.4)
I/σ	11.1 (2.1)	12.6 (4.4)	11.5 (5.2)	11.8 (4.8)

R_{merge} [a]	0.08 (0.54)	0.08 (0.40)	0.08 (0.22)	0.11 (0.57)
		Refinement statistics		
Resolution range, Å	30.28-2.26	53.63-2.27	49.21-1.93	45.56-2.37
Non-hydrogen atoms				
Protein	2031	2055	8080	2031
FAD	53	53	212	53
$NADP^+$	48	48	124	_
2'-P-AMP	_	_	_	27
HTG	19	19	_	19
Solvent	120	35	883	73
R_{work}	0.24	0.24	0.20	0.23
R_{free} [b]	0.27	0.29	0.23	0.27
rmsd bond length, Å	0.014	0.010	0.011	0.010
rmsd bond angles, º	1.9	1.7	1.6	1.5
Average B-factor, $Å^2$	35.1	63.9	14.8	42.9

Values in parentheses correspond to the highest resolution shell.

[a] $R_{sym}=\Sigma|I-I_{av}|/\Sigma I$, where the summatory is over symmetry equivalent reflections.

[b] R calculated for 7 % of data excluded from the refinement.

Table 2. Nucleotide binding and single-turnover kinetic parameters of *R. capsulatus* FPR reaction with NADPH. Values are compared to typical data from plastidic-class FNRs.

Enzyme source	K_d (μM)			k_{obs2} (s^{-1})[a]
	$NADP^+$	2'-P-AMP	NAD^+	
R. capsulatus FPR	222 ± 5	204 ± 4	2,075 ± 45	160
Plastidic-class FNR	5-14[b]	2-15[c]	>10,000 [d]	>380 [e]

[a] Corresponds to the rate constant of hydride transfer between CT-1 and CT-2.

[b] Taken from Batie & Kamin [28], Piubelli *et al.* [32] and Medina *et al*. [7]

[c] Taken from Batie & Kamin [28] and Sancho & Gómez-Moreno [44].

[d] Taken from Arakaki [54].

[e] Taken from Tejero *et al*. [29].

Table 3. B factor values calculated for the models of the native FPR and its complexes obtained with $NADP^+$ y 2'-P-AMP

		Protein B factor values ($Å^2$)	
	Monomer	Complete model	C-terminal
FPR_{FREE}		23.6	24.4
FPR_{NADP}-I		34.7	60.8
FPR_{NADP}-II		63.9	74.5
FPR_{NADP}-III	A	16.0	36.5
	B	13.1*	_
$FPR_{AMP\text{-}2'P}$		42.8	46.9

B factor values calculated for complete model and for the C-terminal tail (residues 268-272) of the polypeptide chain. * C-terminal tail of monomers B and D of the FPR_{NADP}-III complex were modelled until residue 269 and consequently B factor values of the C-terminal tail of the monomer B were not estimated